

CHEM MED CHEM

CHEMISTRY ENABLING DRUG DISCOVERY

Accepted Article

Title: Second generation inhibitors of the mitochondrial permeability transition pore with improved plasma stability

Authors: Justina Sileikyte, Jordan Devereaux, Jelle de Jong, Marco Schiavone, Kristen Jones, Aaron Nilsen, Paolo Bernardi, Michael Forte, and Michael Cohen

This manuscript has been accepted after peer review and appears as an Accepted Article online prior to editing, proofing, and formal publication of the final Version of Record (VoR). This work is currently citable by using the Digital Object Identifier (DOI) given below. The VoR will be published online in Early View as soon as possible and may be different to this Accepted Article as a result of editing. Readers should obtain the VoR from the journal website shown below when it is published to ensure accuracy of information. The authors are responsible for the content of this Accepted Article.

To be cited as: *ChemMedChem* 10.1002/cmdc.201900376

Link to VoR: <http://dx.doi.org/10.1002/cmdc.201900376>

WILEY-VCH

www.chemmedchem.org

A Journal of



FULL PAPER

Second generation inhibitors of the mitochondrial permeability transition pore with improved plasma stability

Dr. Justina Šileikytė^{[a]#}, Dr. Jordan Devereaux^{[b]#}, Jelle de Jong^[d], Dr. Marco Schiavone^[d], Kristen Jones^[a], Dr. Aaron Nilsen^[b], Prof. Paolo Bernardi^[d], Dr. Michael Forte^[a] and Dr. Michael Cohen^{[c]*}

[a] Dr. Justina Šileikytė, ORCID: 0000-0002-6795-6344, Kristen Jones and Dr. Michael Forte
Vollum Institute
Oregon Health and Science University
3181 SW Sam Jackson Park Road, Portland, OR 97239

[b] Dr. Jordan Devereaux and Dr. Aaron Nilsen
Medicinal Chemistry Core
Oregon Health and Science University
3181 SW Sam Jackson Park Road, Portland, OR 97239

[c] Dr. Michael Cohen, ORCID: 0000-0002-7636-4156
Department of Chemical Physiology & Biochemistry
Oregon Health and Science University
3181 SW Sam Jackson Park Road, Portland, OR 97239
E-mail: cohenmic@ohsu.edu

[d] Jelle de Jong, Dr. Marco Schiavone and Prof. Paolo Bernardi
Department of Biomedical Sciences
University of Padova
Via Ugo Bassi 58/B, I-35131 Padova (Italy)

Justina Šileikytė and Jordan Devereaux equally contribute to this work.

* Corresponding Author

Supporting information for this article is given via a link at the end of the document.

Abstract: Excessive mitochondrial matrix Ca^{2+} and oxidative stress leads to the opening of a high-conductance channel of the inner mitochondrial membrane referred to as the mitochondrial permeability transition pore (mtPTP). Because mtPTP opening can lead to cell death under diverse pathophysiological conditions, inhibitors of mtPTP are potential therapeutics for various human diseases. High throughput screening efforts led to the identification of a 3-carboxamide-5-phenol-isoxazole compounds as mtPTP inhibitors. While they showed nanomolar potency against mtPTP, they exhibited poor plasma stability, precluding their use in *in vivo* studies. Herein, we describe a series of structurally related analogs in which the core isoxazole was replaced with a triazole, which resulted in an improvement in plasma stability. These analogs were readily generated using the copper-catalyzed “click chemistry”. One analog, *N*-(5-chloro-2-methylphenyl)-1-(4-fluoro-3-hydroxyphenyl)-1*H*-1,2,3-triazole-4-carboxamide (**TR001**), was efficacious in a zebrafish model of muscular dystrophy that results from mtPTP dysfunction whereas the isoxazole isostere had minimal effect.

Introduction

Cellular Ca^{2+} metabolism and bioenergetics function as an integrated system, which is reflected by the mitochondrion's high capacity to store Ca^{2+} in response to signals arising from elevated cytoplasmic Ca^{2+} [1,2]. While a number of specific mitochondrial Ca^{2+} uptake and release pathways have been defined, the mitochondrial permeability transition pore (mtPTP) represents a unique kind of mitochondrial Ca^{2+} release pathway. Indeed, this route of mitochondrial Ca^{2+} release is characterized as a voltage-dependent, cyclosporin A (CsA)-sensitive, high-conductance

channel of the inner mitochondrial membrane (IMM) activated by mitochondrial accumulation of Ca^{2+} , but is not selective for Ca^{2+} [3]. Many structurally unrelated compounds or conditions affect mtPTP transitions between its open and closed conformation; and the identification of numerous, discrete regulatory mechanisms strongly suggest a molecular structure of pronounced complexity [4-6]. mtPTP plays a key role in many diverse human pathologies whose shared characteristics may be based in mitochondrial dysfunction triggered by Ca^{2+} and potentiated by oxidative stress (e.g., [7]). However, the molecular composition of the mtPTP has been historically distracted by assumptions that had little experimental evidence and have subsequently been discounted from their participation in mtPTP formation through rigorous genetic analysis (e.g., [8]). More recently, a novel hypothesis proposes that the mtPTP forms from dimers of the F_0F_1 -ATP synthase (ATP synthase) [9]. However, alternate models have been developed [10]; as a result, the identity of the proteins forming the mtPTP are currently debated.

The identification of pharmacological agents that specifically inhibit the mtPTP would provide key insights into its molecular composition. Pharmacological agents targeting the mtPTP generally target regulatory factors, not mtPTP itself. For example CsA targets cyclophilin D (CyPD), an essential regulator of mtPTP [3]. An inherent limitation of CsA and other CyPD inhibitors is that these compounds are not mtPTP blockers, as demonstrated by the fact that the mtPTP can still open after genetic elimination of CyPD (e.g., [11]). Recently we identified several classes of compounds that specifically target the mtPTP using robust, high throughput mtPTP assays [12,13]. We identified several chemotypes that were optimized using medicinal chemistry efforts to yield, to our knowledge, the most potent mtPTP inhibitors

FULL PAPER

reported to date. These mtPTP inhibitors—the most potent of which contain an isoxazole core—are efficacious at nanomolar concentrations, are non-toxic in mammalian cells and are efficacious in an animal model of a human muscular dystrophy caused, in part, by pathological mtPTP activation. However, plasma instability of the isoxazole-based mtPTP inhibitors limited further *in vivo* studies. Thus, we sought improvement of plasma stability of these mtPTP inhibitors. Herein, we describe a new series of triazole-based mtPTP inhibitors that exhibit improved plasma stability. The synthesis of the triazole core of these inhibitors was accomplished using “click chemistry” of easily prepared aryl azides and aryl propynamides. The facile synthesis of the triazole mtPTP inhibitors facilitated thorough structure-activity relationship (SAR) studies. In a zebrafish model of muscular dystrophy caused by inappropriate mtPTP activation, the triazole-based inhibitor **TR001** was more efficacious than the nearly identical isoxazole-based inhibitor **63**.

Results and Discussion

Plasma stability of first generation mtPTP inhibitors

The first generation of mtPTP inhibitors described by Roy *et al.*^[12] contain a core heterocycle flanked by two aryl substituents. The most potent compound, **63**, has isoxazole with a carboxamide at C-3 and an *ortho* substituted phenol group at C-5 (Table 1). While it exhibits nanomolar potency against mtPTP *in vitro*, it has a short half-life ($t_{1/2}$) in plasma ($t_{1/2}$ of 21 minutes, Table 1). Replacing the isoxazole with either a pyrazole (**72**) or an *N*-2-methyl pyrazole (**73** and **74**) improved plasma stability (Table 1), but unfortunately these compounds exhibited mitochondrial toxicity^[12].

Synthesis of triazole analogs

Previous studies demonstrated that replacement of an isoxazole core with a triazole in TGR5 agonists resulted in a substantial improvement in pharmacokinetic properties^[14]. Because we desire mtPTP inhibitors with favorable pharmacokinetic profiles for *in vivo* studies, we designed and synthesized a series of second generation analogs of **63** in which the core isoxazole was replaced with a triazole. These analogs exhibit various substituents on the phenolic group at N-1 position of the triazole ring for exploring SAR on this side of the compounds.

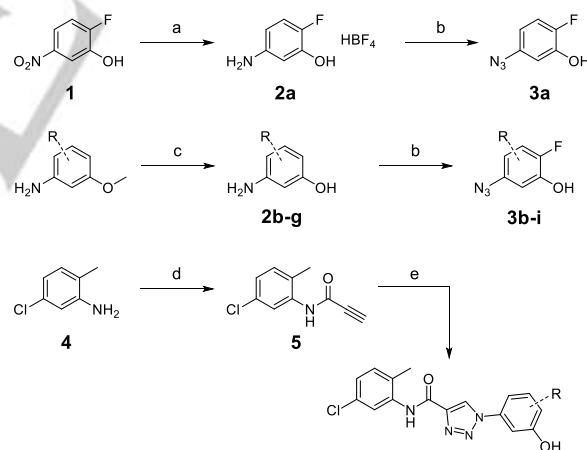
The synthesis of these compounds is described in Scheme 1. Briefly, 1,3-Aminophenols **2a-i** were purchased or synthesized from aryl nitro or aryl methoxy starting materials. These anilines were diazotized using a method adapted from Filimonov^[15], then subsequently converted into aryl azides **3a-i** using standard procedures. Aniline **4** was coupled to propionic acid using standard DCC coupling procedures to afford the *N*-phenyl propiolamide **5**. Finally, triazoles **TR001-013** were synthesized readily by coupling the aryl azides **3a-i** to *N*-phenyl propiolamide **5** using the copper(I)-mediated Huisgen cycloaddition reaction (commonly referred to as “click chemistry”).

Table 1. The central heterocyclic core of mtPTP inhibitors impacts mouse plasma stability.

Compound	Structure	Mouse Plasma $t_{1/2}$ (min)
TR001		990
63 ^[a]		21
72 ^[a]		533
73 ^[a]		85
74 ^[a]		151

[a] Compounds first reported in^[12].

Initially, we evaluated the plasma stability of **TR001**. Compared to **63**, **TR001** exhibited a 47-fold increase in plasma stability (Table 1). This result demonstrates that substantial improvement in plasma stability can be achieved by simply replacing the isoxazole in **63** with a triazole.



Scheme 1. General synthetic procedure for triazole analogs. Reagents: (a) Pd/C, HBF₄•Et₂O, H₂, MeOH; (b) 1 - NaNO₂, HBF₄•Et₂O, AcOH, 2- NaN₃, H₂O, EtOAc; (c) BBr₃, DCM; (d) DCC, MeCN; (e) 3b-i, CuSO₄•5 H₂O, sodium ascorbate, EtOH.

Structure-activity relationship studies

We next sought to evaluate the effects of **TR001-13** on mtPTP activity *in vitro* in isolated mitochondria. In isolated mitochondria, induction of mtPTP opening leads to mitochondrial swelling due to the oncotic pressure gradient created by matrix proteins >1.5 kDa that cannot diffuse through

FULL PAPER

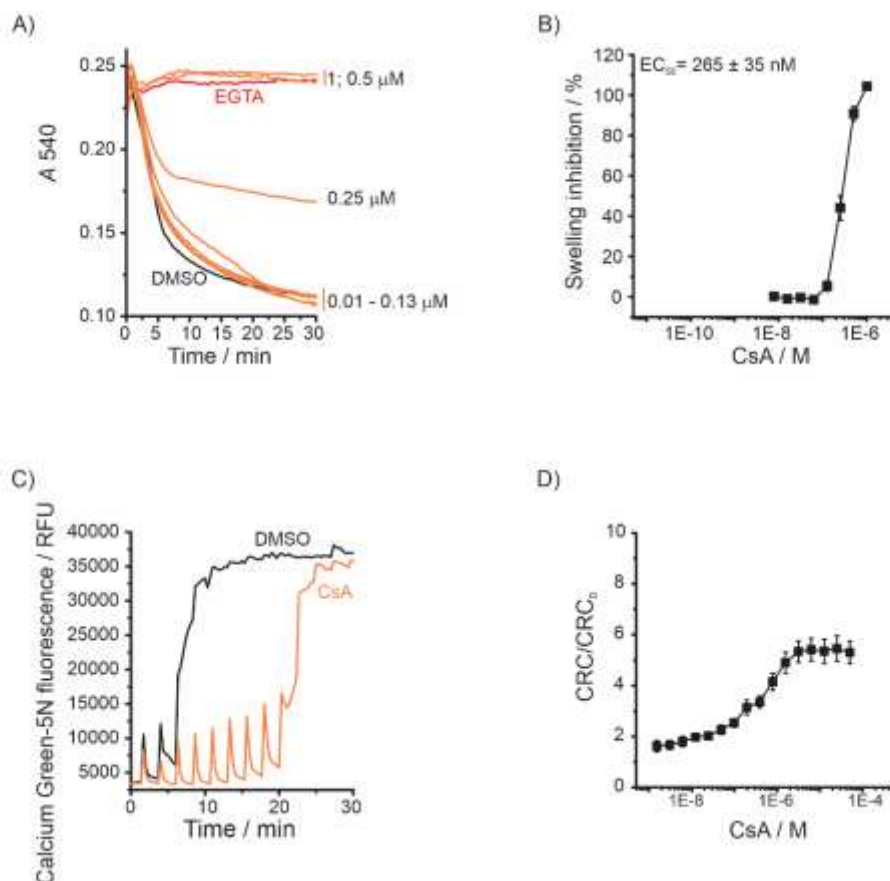


Figure 1. CsA, an established mtPTP inhibitor, prevents mitochondrial swelling. A) Representative traces of effect of indicated concentrations of CsA on Ca^{2+} overload ($60 \mu\text{M}$) induced mitochondrial swelling in isolate mouse liver mitochondria. B) Percent of inhibition was calculated at 20 min after Ca^{2+} addition. Data are average \pm SEM of $n=39$ independent preparations. C) Representative traces of calcium retention capacity (CRC) of vehicle (DMSO) or $1.25 \mu\text{M}$ CsA treated mouse liver mitochondria. Each spike of fluorescence represents $10 \mu\text{M}$ Ca^{2+} injection. D, Concentration response of compound treated, CRC, to DMSO-treated, CRC_0 , ratios, data are average \pm SEM of $n=25$ independent preparations.

the open pore. In *in vitro* experiments, where isolated mitochondria are routinely suspended in sucrose-based isotonic solutions, the change in mitochondrial size can be measured spectrometrically by detecting the decrease in light scattering at 540 nm.

First, we sought to confirm that the established mtPTP inhibitor CsA prevents mitochondrial swelling in the expected concentration range in our mitochondrial preparations. We challenged isolated mouse liver mitochondria with $60 \mu\text{M}$ Ca^{2+} to induce mtPTP opening in the presence of vehicle (DMSO) or increasing concentrations of CsA. As expected, CsA dose-dependently reversed the Ca^{2+} -mediated decrease in light scattering (EC_{50} value of $265 \pm 35 \text{ nM}$) (Figure 1 A, B).

Next, we used the Ca^{2+} retention capacity (CRC) assay to validate the activity of CsA. CRC determines the Ca^{2+} threshold required for mtPTP activation; inhibitors of mtPTP are expected to increase the Ca^{2+} threshold required for mtPTP induction. Extramitochondrial Ca^{2+} changes are detected using the membrane-impermeant Ca^{2+} indicator, Calcium Green-5N. Consistent with previous studies, CsA increased the Ca^{2+} load mitochondria could store before mtPTP opening (from ~ 70 to $320 \text{ nmol/mg protein}$), with a CRC ratio (drug-to-vehicle) of 4.6 at $1.25 \mu\text{M}$ CsA (Figure 1 C, D).

We next determined the swelling EC_{50} and CRC ratios for **TR001-013** (Figure 2 and Table 2). Out of 13 compounds tested four compounds showed superior activity, one comparable

activity and eight lower activity (or were inactive) compared to CsA (Figure 2).

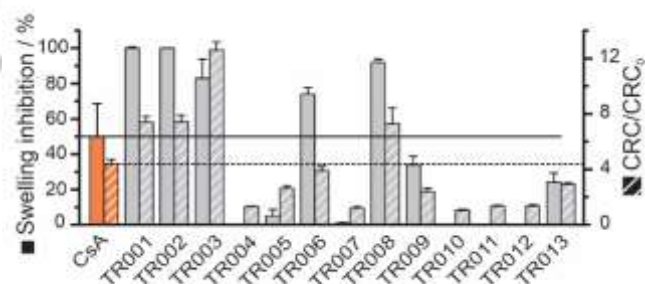


Figure 2. Triazole-based mtPTP inhibitors prevent mitochondrial swelling. ■, Percent of Ca^{2+} overload induced mitochondrial swelling inhibition at 265 nM of indicated compounds; data are average \pm SEM of $n=3-41$ independent preparations. ▒, ratios of calcium retention capacity (CRC) at $1.25 \mu\text{M}$ compound, i.e., concentration at which CsA reaches its full efficacy, treated mitochondria to DMSO (CRC_0) treated mitochondria; data are average \pm SEM of $n=3-25$ independent preparations.

While the majority of the substituents on the phenolic ring of the isoxazole series^[12] had been *ortho* to the hydroxyl group, it was unclear whether this was optimal for mtPTP inhibitory activity. Because of the readily available starting materials and facile synthetic route we developed for the triazole series, we could easily test the effects of *ortho* versus *meta* versus *para* substitution on the phenolic ring. A series of isobaric compounds

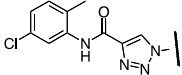
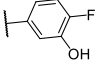
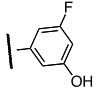
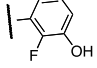
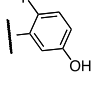
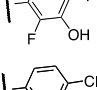
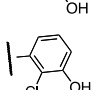
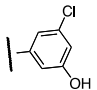
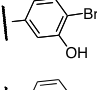
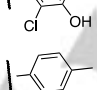
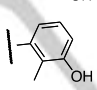
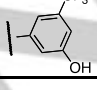


FULL PAPER

were prepared which contain a fluorine at all three positions in the phenolic ring. The most potent analog was the *meta* substituted compound **TR002** followed by *ortho* analog **TR001** (Table 2).

Interestingly, the alternative *ortho* analog **TR003** exhibited a 5-fold decrease in activity compared to **TR001** and the *para* analog **TR004** was inactive (Table 2). The difluoro analog **TR005** with substitutions at both *ortho* positions exhibited decreased activity (Table 2). These results suggest that the position of the fluorine substituent can dramatically influence activity on mtPTP, and

support very tight steric and electronic constraints on inhibitor binding to its target.

We also synthesized analogs that contain other substituents on the phenolic ring to further explore the SAR. Analogs of **TR001** with either chlorine (**TR006**) or bromine (**TR009**) in the *ortho* position exhibited decreased activity and CRC/CRC₀ ratio compared to **TR001** (Table 2). Similar results were found for the chlorine analog of **TR002** (**TR008**) which exhibited a 2-fold decrease in activity

Compound		Mitochondrial Swelling EC ₅₀ (μM) ^[a]	CRC/CRC ₀ at 1.25 μM ^[b]	Rh123 uptake EC ₅₀ (μM) ^[c]	Table 2. Structure- activity relationships of triazole analogs.
TR001		0.029 ± 0.008	6.8 ± 0.4	> 40	
TR002		0.010 ± 0.002	12.6 ± 0.6	14.1 ± 1.2	
TR003		0.152 ± 0.036	7.4 ± 0.5	29.3 ± 3.3	
TR004		> 20	1.3 ± 0.03	> 40	
TR005		0.782 ± 0.114	2.6 ± 0.2	> 40	
TR006		0.135 ± 0.015	3.9 ± 0.3	> 40	
TR007		> 20	1.2 ± 0.1	> 40	
TR008		0.028 ± 0.005	7.3 ± 1.1	> 40	
TR009		0.475 ± 0.057	2.4 ± 0.2	> 40	
TR010		> 20	1.1 ± 0.1	> 40	
TR011		> 20	1.4 ± 0.1	> 40	
TR012		10.6 ± 1.4	1.4 ± 0.1	> 40	
TR013		0.534 ± 0.047	2.9 ± 0.1	6.2 ± 1.2	

FULL PAPER

[a] Data are average \pm SEM of $n=3-41$ independent preparations. [b] Compound treated mitochondrial calcium retention capacity (CRC) to DMSO treated (CRC₀) ratios. Data are average \pm SEM of $n=3-25$ independent preparations. [c] Interference with rhodamine 123 (Rh123) uptake to mitochondria as a readout of interference with a buildup of inner mitochondrial membrane potential. Data are average \pm SEM of $n=3$ independent preparations.

WILEY-VCH

Accepted Manuscript

FULL PAPER

compared to **TR002** (Table 2). The methyl substituted analogs **TR011** and **TR012** were inactive, suggesting a preference for electron withdrawing groups on the phenolic ring. Interestingly, however, the trifluoromethyl analog **TR013** had significantly reduced activity compared to either **TR002** or **TR008**, suggesting that the steric bulk is a greater influence than electronics.

We next evaluated the mitochondrial toxicity of the new triazole analogs by testing their ability to interfere with accumulation of the membrane-permeant cationic fluorescent dye rhodamine 123 (Rh123). The mitochondrial uptake of positively charged Rh123 is driven by the negative IMM potential inside mitochondria, which is generated by the respiratory chain or maintained by ATP hydrolysis if certain conditions are met. The majority of triazoles does not interfere with the buildup of IMM potential except for **TR002**, **TR003** and **TR013** (Table 2). Hence the position and nature of the substituent on the phenolic ring can influence mitochondrial toxicity. It should be noted, however, that toxicity for these compounds only occurs at ~ 10 – 1000-fold higher concentrations compared to mtPTP inhibition.

TR001 is a potent inhibitor of the mtPTP

Based on the SAR studies and mouse plasma stability data, we decided to move forward with **TR001** for more extensive biological characterization. As noted above, mtPTP is triggered by elevated levels of matrix Ca^{2+} and potentiated by oxidative stress, leading to mitochondrial swelling. We therefore next tested the ability of **TR001** to protect from oxidizing agent-triggered mtPTP opening. For this purpose, we used known chemical activators of the mtPTP that react with two distinct classes of redox sensitive protein thiols and increase mtPTP opening. We first pretreated energized isolated mouse liver mitochondria with $10\ \mu\text{M}\ \text{Ca}^{2+}$, an amount insufficient to induce mtPTP opening (Figure 3 A-D, traces a). We then then added (i) phenylarsine oxide (PhAsO) or Diamide (Figure 3 A and B, respectively), reagents that primarily react with matrix thiols^[16] or (ii) copper-*o*-phenanthroline ($\text{Cu}(\text{OP})_2$) and *N*-ethylmaleimide (NEM) (Figure 3 C and D, respectively), reagents that react with intermembrane space exposed thiols^[17,18], to induce mtPTP transition from a closed to open conformation (Figure 3 A-D, traces b). Samples were treated either with $1.5\ \mu\text{M}\ \text{CsA}$ or $1.5\ \mu\text{M}\ \text{TR001}$ prior to Ca^{2+} and oxidant addition. In all cases both CsA and **TR001** delayed mtPTP opening, with **TR001** being much more effective than CsA .

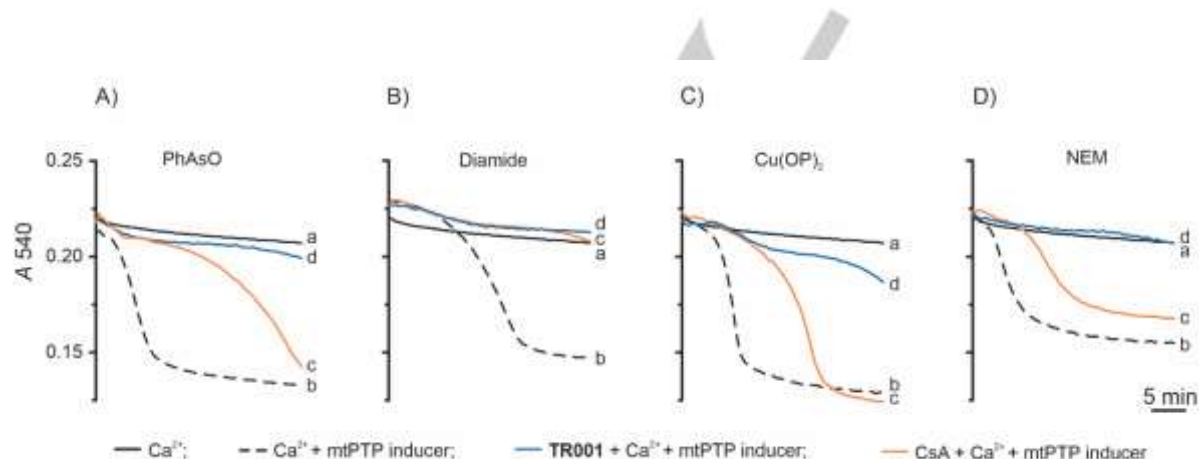


Figure 3. **TR001** prevents chemical activation induced mitochondrial swelling. A-D) mouse liver mitochondria ($0.25\ \text{mg/mL}$) were treated with $10\ \mu\text{M}\ \text{Ca}^{2+}$ only (traces a); $10\ \mu\text{M}\ \text{Ca}^{2+}$ and after 2 min of incubation with: A) $7\ \mu\text{M}\ \text{PhAsO}$, B) $2\ \text{mM}\ \text{Diamide}$, C), $7\ \mu\text{M}\ \text{Cu}(\text{OP})_2$, D), $2\ \text{mM}\ \text{NEM}$ (traces b-d). In traces c and d additions were as in traces b except that mitochondria were also treated with $1.5\ \mu\text{M}\ \text{CsA}$ (traces c) or **TR001** (traces d). Traces are representative of $n=4$ independent preparations.

CyPD is not a target of TR001

The above experiments demonstrate that **TR001** is a more potent mtPTP inhibitor than CsA . We next asked if **TR001** acts on a different target than CsA . We found that **TR001** was additive with CsA (Figure 4 A), supporting the notion that **TR001** and CsA act on different targets. To directly determine if **TR001** acts on

CyPD,— the target of CsA ,—we performed the CRC test in permeabilized WT or CypD-null HEK 293T cells. In contrast to CsA , which had no effect on CypD-null cells, **TR001** increased the CRC in both WT and CypD-null cells (Figure 4 B). Taken together, these results provide strong evidence that CyPD is not the target of **TR001**.

FULL PAPER

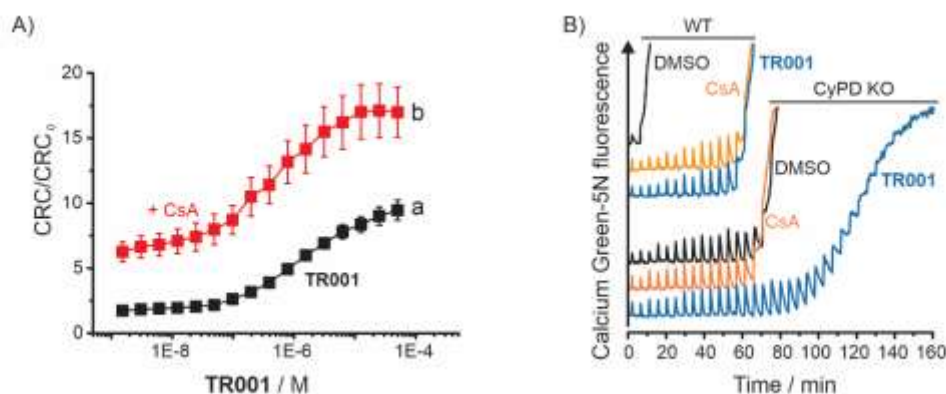


Figure 4. TR001 inhibits the mtPTP independently of CyPD. A, CRC ratios of mouse liver mitochondria treated with TR001 only (trace a) or in combination with 2 μM CsA (trace b). Data are average ± SEM of 7 and 5 independent preparations, respectively. B, CRCs of permeabilized HEK293T WT or CyPD KO cells treated with DMSO, 10 μM CsA or 10 μM TR001. Each spike in fluorescence indicates 10 μM Ca²⁺ injection. Traces are representative of 4 independent preparations.

TR001 does not affect mitochondrial or cultured cell health

A thorough evaluation of toxicity is critical for advancing TR001 for *in vivo* studies. Initial assessment using the Rh123 uptake assay showed that TR001 did not interfere with IMM potential. To more thoroughly examine mitochondrial toxicity, we analyzed oxygen consumption rates (OCRs) using the Seahorse XF24 extracellular flux analyzer. This allowed us to assess the effects of TR001 on mitochondrial respiration and ATP synthesis. We found that TR001 had no effect on rates of oxygen consumption upon ADP stimulation (ATP production), after ATP synthase inhibition with oligomycin (basal respiration), or uncoupling with FCCP (maximal respiratory capacity) in isolated

mitochondria (Figure 5 A). Consequently respiratory control ratios (i.e., the ratios between ADP-stimulated and basal respiration) were not affected up to 50 μM TR001 (Figure 5 B). Complex III inhibitor antimycin A shuts down the electron transport chain at the bc1 complex and was used to account for oxygen leak. Similar results were obtained in intact cells (i.e., TR001 did not cause mitochondrial dysfunction in the course of ~ 2 h treatment) (Figure 5 C). Finally, TR001 (up to 50 μM) did not exhibit any adverse effects on HeLa cell viability (Figure 5 D). Together, these results demonstrate that the TR001 is not toxic to mitochondria or cells.

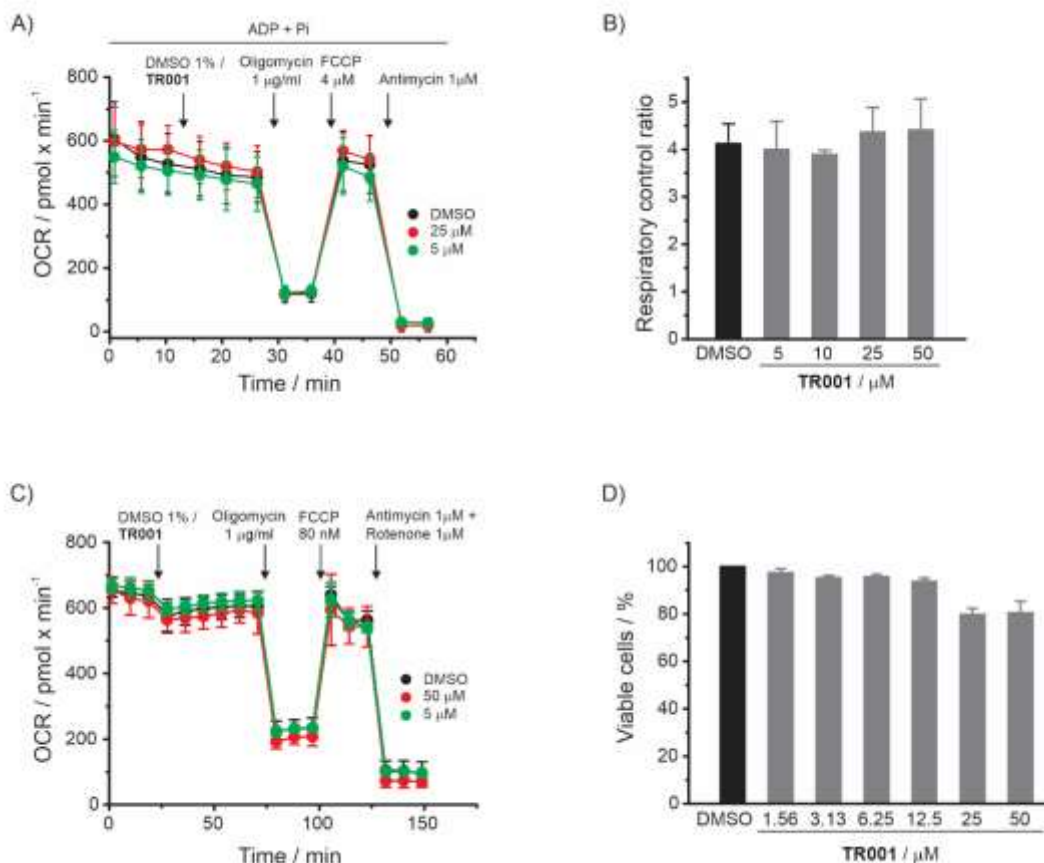


Figure 5. TR001 is not toxic to either mitochondria or intact cells. Oxygen consumption rates (OCR) of isolated mitochondria, A, or HeLa cell monolayers, C, were measured in the presence of indicated concentrations of TR001. Traces are representative of 4 and 5 separate experiments, respectively. B, Respiratory control

FULL PAPER

ratios of isolated mitochondria. D, Interference with HeLa cell proliferation after 24 h treatment with **TR001**. B and D, data are average \pm SEM of 4 and 6 independent experiments.

Assessment of the therapeutic potential of **TR001** in a vertebrate model of mtPTP-based disease

Long-lasting opening of the mtPTP, likely due to mitochondrial Ca^{2+} overload^[19], is a common downstream mechanism during the pathogenesis of several muscular dystrophies, like Ullrich Congenital Muscular Dystrophy (UCMD). This is a life-threatening disorder caused by mutations in genes encoding collagen VI. These mutations result in defective or absent collagen VI, an essential component of extracellular matrix in skeletal muscle. Mouse models of UCMD with knock-outs for the murine *Col6a1* gene exhibit relatively mild phenotypes when compared to those observed in humans. However, it is widely documented that inappropriate mtPTP activity, both in humans and mice, plays a key role in disease pathogenesis^[20–22]. Desensitization of the mtPTP both in mice and human cell lines, using either pharmacological treatment with CyP inhibitors (CsA and its non-immunosuppressive derivatives)^[20,23] or elimination of the *Ppif* gene encoding CyPD^[21] were found to restore normal mitochondrial function and to decrease myofiber cell death. An additional model of UCMD has been generated in zebrafish through the injection of an antisense morpholino oligonucleotide directed to the exon 9 splicing region of the human orthologous *col6a1* gene in zebrafish, resulting in an in-frame deletion mimicking common mutations in human UCMD^[24,25]. Morpholino-injected animals (morphants) developed a severe myopathy which accurately mimicked the clinical severity of human UCMD with early-onset motor deficits and severe muscular and mitochondrial ultrastructural changes. This severe phenotype was reversed by treatment with non-immunosuppressive derivatives of CsA^[25]. Thus, we used the zebrafish *col6a1* myopathic morphant as a powerful in vivo system to validate the therapeutic potential of **TR001** and compared it to the isoxazole compound **63** which exhibits similar potency to **TR001**, but substantially decreased plasma stability (Table 1).

Zebrafish embryos were injected with *col6a1* morpholino at the 1-cell stage, dechorionated at 20 hours post fertilization (hpf) and treated at 21 hpf with 0.1, 1 or 10 μM of either **TR001** or **63**. DMSO-treated embryos injected with a scrambled morpholino were used as a control. Motor deficits due to a delay in muscle fiber development were evaluated by measuring both spontaneous contractions and swimming abilities at early stages of embryo development when the muscles are not fully developed. Spontaneous coiling events were monitored at 24 hpf after 3 hours of inhibitor treatment. *col6a1* morphants exhibited a substantial decrease in the number of spontaneous coiling events compared to zebrafish injected with a scrambled morpholino and treated with vehicle (Figure 6 A). Treatment with **TR001** partially

rescued the defect observed in *col6a1* morphants in a dose-dependent manner; in contrast, **63** had no effect (Figure 6 A). We next evaluated touch-evoked escape responses to determine the ability of zebrafish embryos to start swimming after a mechanical stimulus. Touch-evoked escape responses were measured 48 hpf, (27 hours of treatment with inhibitor). *col6a1* morphants showed a severely reduced motility, which was improved by treatment with **TR001** (Figure 6 B). By contrast, treated with **63** resulted in minimal recovery at 0.1–1.0 μM , an effect that was no longer seen at 10 μM (Figure 6 B). It should be noted that in these protocols, embryos were exposed to drugs for a longer period of time than in the spontaneous coiling experiments. This difference explain why **TR001** was as effective at 0.1 μM as it was at 1 and 10 μM .

Muscle structure was assessed by birefringence analysis at 48 hpf, a time when muscle tissue is fully developed and organized muscle fibers start to show anisotropic features. A high percentage of severe birefringence abnormality (>75%, Figure 6 C) was detected in *col6a1* morphants, indicating major defects of muscle fiber development and organization. **TR001** significantly rescued this defect in muscle structure in *col6a1* morphants whereas **63** exhibited a minimal effect (Figure 6 C).

To test the effects of both **TR001** and **63** on the respiration of *col6a1* morphant embryos, we measured the OCR on entire embryos at 48 hpf. Sequentially, we measured (i) the basal respiration, (ii) the coupled respiration through the addition of 10 μM oligomycin which inhibits the activity of ATP Synthase, (iii) the maximal respiratory capacity by adding 2 μM of the uncoupler FCCP, and (iv) the mitochondrial respiration after the inhibition of Complexes I and III by adding 1 μM rotenone and 1 μM antimycin A. We found that respiration of *col6a1* morphants (closed squares) was significantly lower ($p < 0.001$) than that of embryos injected with scrambled morpholino (open squares) (Figure 6 D). Moreover, **TR001** at a concentration of 10 μM was able to fully restore the maximal respiratory capacity (Figure 6 D, left panel, open diamonds, $p < 0.001$) of *col6a1* morphants. In general, **TR001** at all concentration used (Figure 6 D, left panel) was more effective than **63** (Figure 6 D, right panel).

Lastly, fish survival was also assessed. Fifty percent of *col6a1* morphant embryos treated with 0.1 μM of **TR001** survived 7 days longer than *col6a1* morphants treated with DMSO ($p < 0.0001$ from 3 to 12 dpf), and 20% were still alive at 30 dpf (29 days of treatment) (Figure 6 E). Moreover, treatment with 1 μM **TR001** was also effective at improving survival rate of *col6a1* morphants ($p < 0.01$ from 3 to 12 dpf), while 10 μM **TR001** was ineffective. The lowest concentration of **63** tested showed decreased activity compared to **TR001** and the rest were ineffective (Figure 6 E).

FULL PAPER

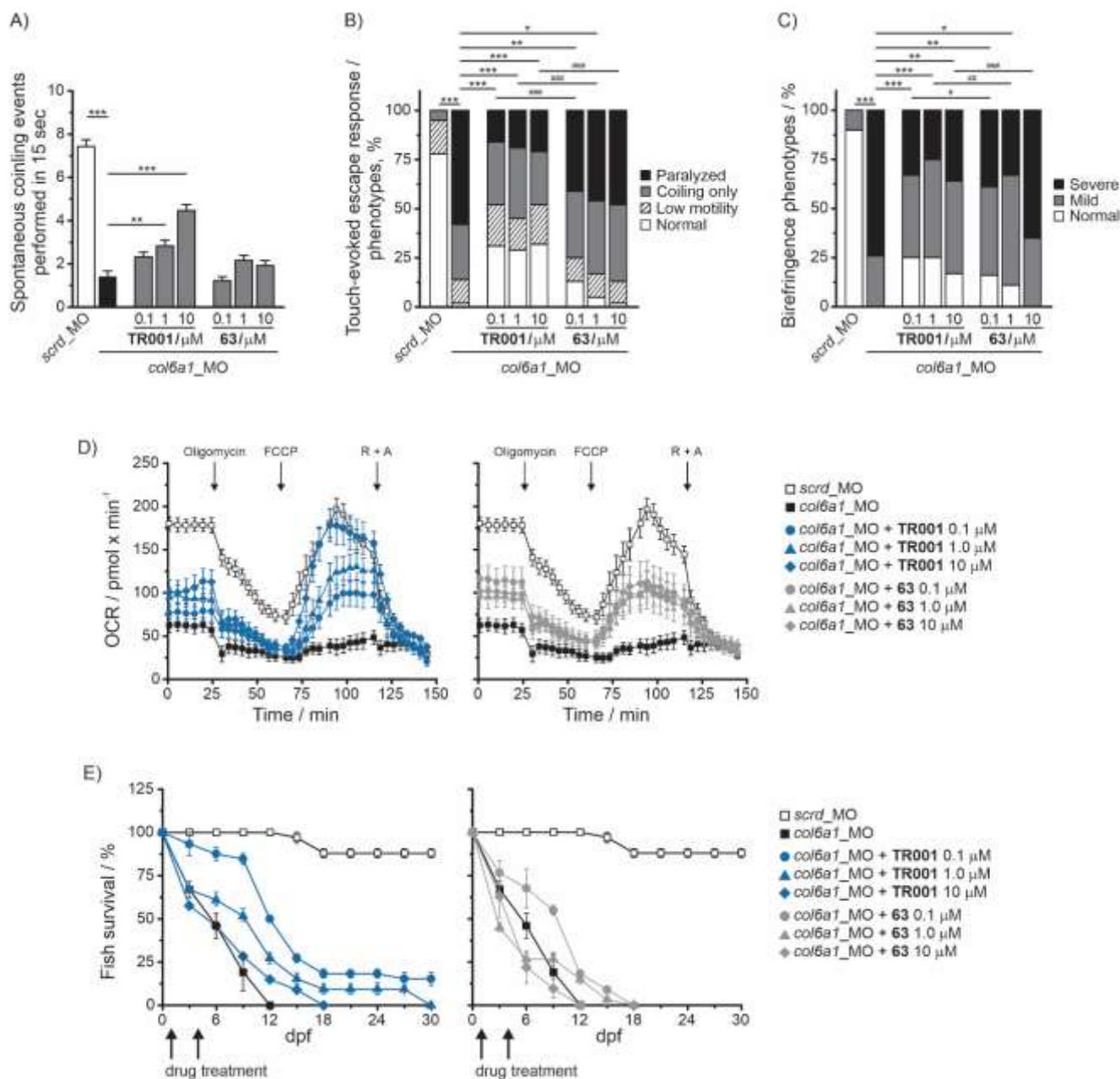


Figure 6. TR001, but not 63, showed efficacy in a zebrafish model of a muscular dystrophy based on dysregulation of the mtPTP. A, Spontaneous coiling events were recorded at 24 hpf in DMSO-treated zebrafish injected with the scrambled morpholino (*scrd_MO*), DMSO-treated *col6a1* morphants (*col6a1_MO*) and *col6a1* morphants (*col6a1_MO*) treated with the indicated concentrations of TR001 or 63. Data report the number of spontaneous coiling events in 15 seconds and are reported as mean \pm SEM of 6 independent experiments ($n=52$ for each condition); ** $p < 0.01$, *** $p < 0.001$ as analyzed by one-way ANOVA with Bonferroni correction. B, Touch-evoked escape responses were recorded at 48 hpf. Embryos were divided in four sub-groups according to the phenotype observed: paralyzed (black bar), coiling only (gray bar), low motility (hatched bar) and normal (white bar). Data are reported as percentage of these phenotypes per each treatment condition. Comparison between groups were made using χ^2 test and one-way ANOVA with Bonferroni correction; # $p < 0.05$, ## $p < 0.01$, ### $p < 0.001$. The symbol * is for statistical analysis comparing DMSO-treated *col6a1* morphants (*col6a1_MO*) and those treated with increasing doses of both TR001 and 63; the symbol # is used for statistical analysis comparing the two groups of *col6a1_MO* treated with TR001 or 63. Six independent experiments were performed. C, Birefringence was measured at 48 hpf and zebrafish embryos were divided in 3 subgroups according to the phenotype observed: normal (white bar), mild (gray bar) and severe (black bar) phenotype. Four independent experiments were performed and the final number of zebrafish embryo per group was 40 for each condition. Data are reported as the percentage of birefringence phenotypes. Data were analyzed by using χ^2 test and one-way ANOVA with Bonferroni correction; # $p < 0.05$, ## $p < 0.01$, ### $p < 0.001$. D, oxygen consumption rate (OCR) was measured on entire zebrafish embryos at 48 hpf. Left panel represents data from embryos injected with a scrambled morpholino (*scrd_MO*, \square), *Exon 9 col6a1* morpholino (*col6a1_MO*, \blacksquare) and *col6a1_MO* embryos treated with TR001 at 0.1 μ M (\bullet), 1.0 μ M (\blacktriangle), 10 μ M (\blacklozenge). Right panel represents data from embryos injected with a scrambled morpholino (*scrd_MO*, \square), *Exon 9 col6a1* morpholino (*col6a1_MO*, \blacksquare) and *col6a1_MO* embryos treated with 63 at 0.1 μ M (\bullet), 1.0 μ M (\blacktriangle), 10 μ M (\blacklozenge). Embryos were treated with oligomycin, FCCP, rotenone (R) and antimycin A (A) as indicated. Results are presented as mean \pm SEM. Both graphs report data from 5 independent experiments with $n=20$ for each treatment. Error bars are reported as SEM. E, Survival of DMSO-treated zebrafish injected with the scrambled morpholino (\square), DMSO-treated *col6a1* morphants (\blacksquare) and *col6a1* morphants treated with: left panel, TR001 (0.1 μ M, \bullet ; 1.0 μ M, \blacktriangle ; 10 μ M, \blacklozenge) or right panel, 63 (0.1 μ M, \bullet ; 1.0 μ M, \blacktriangle ; 10 μ M, \blacklozenge) were recorded for 30 days. Treatment started at 21 hpf and repeated at 4 dpf (arrows). Data report the percentage of surviving fish and are mean \pm SEM from 3 independent experiments ($n=15$ for each condition in each set).

FULL PAPER

Conclusions

In this study, we demonstrate that replacing the core isoxazole in our previously described mtPTP inhibitor **63** with a triazole (**TR001**) results in improved plasma stability while maintaining potent mtPTP inhibition. Because the triazole analogs could be generated in a facile manner, we were able to perform SAR studies focused on the effects of substituents on phenolic ring at N-1 of the triazoles. These studies revealed a tight SAR, with a preference for a fluorine at the *ortho* or *meta* position of the phenolic ring. The tight SAR suggests that the phenolic ring projects into a well-defined pocket on a yet-to-be-identified target. The SAR studies performed in this study will guide the development of analogs for target identification. Finally, we demonstrated in an animal model of a muscular dystrophy based on dysregulation of the mtPTP the triazole **TR001** is more efficacious than the sterically equivalent isoxazole **63**. Our studies guide the further development of these compounds as potential therapies for a wide variety of human pathologies in which dysfunction of the mtPTP plays a key role.

Experimental Section

Chemistry

5-amino-2-fluorophenol tetrafluoroborate. 1 (2.5 g, 16 mmol) was dissolved in 80 mL of EtOH. Tetrafluoroboric acid etherate (4.35 mL, 32 mmol) and Pd/C (10% w/v, 0.25 g) were added, then the mixture was placed under a hydrogen atmosphere (20 psi) for 18 hr with shaking. The Pd/C was removed by filtration over celite, then the solution was concentrated to give 3.357 g of **2a** (98% yield). ¹H NMR (d₆-DMSO) δ 10.49 (s, 1H); 9.64 (s, 3H); 7.25 (q, 1H); 6.93 (q, 1H); 6.73 (m, 1H).

5-azido-2-fluorophenol. 2a (1.655 g, 7.7 mmol) was dissolved in 15 mL of AcOH. Tetrafluoroboric acid etherate (2.62 mL, 19.2 mmol) was added, followed by sodium nitrite (0.8 g, 11.5 mmol) in three portions over 30 min. The mixture was added dropwise to 150 mL of vigorously stirring Et₂O at 0° C. The resulting light brown precipitate was collected by filtration, then used in the next step without further purification. Sodium azide (5 g, 77 mmol) was dissolved in 77 mL of H₂O at 0° C. The diazonium from step 1 was added and stirred for 15 min at 0° C. The reaction was extracted 3X with 25 mL of EtOAc. The organic fractions were combined, washed 2X with 10 mL of brine, then dried with MgSO₄, filtered, and concentrated to give 0.97 g of **3a** (82% yield). ¹H NMR (d₆-DMSO) δ 10.28 (q, 1H); 7.18 (m, 1H); 6.66 (q, 1H); 6.54 (m, 1H).

General procedure for BBr₃ demethylation. A flask was loaded with molecular sieves (3Å) and flame dried under vacuum. After cooling under argon, starting methyl ether (2 mmol) was loaded, followed by 10 mL of dry DCM. The flask was sealed and degassed, then the solution was cooled to -78° C. BBr₃ (0.9 mL, 10 mmol) was added dropwise, then the reaction was stirred for 18 hr to RT. The reaction was decanted into excess aqueous sat. sodium bicarbonate, then extracted 3X with 20 mL of EtOAc. The organic fractions were combined, washed 2X with 20 mL of brine, then dried with MgSO₄, filtered, and concentrated to give product in 20% to quantitative yield.

3-amino-2-fluorophenol (2b). Quant. yield. ¹H NMR (CDCl₃) δ 6.81 (m, 1H); 6.38 (m, 2H); 5.02 (s, 1H); 3.75 (s, 2H).

3-amino-5-fluorophenol (2c). 20% yield. ¹H NMR (d₆-DMSO) δ 9.28 (s, 1H); 5.81 (d, 1H); 5.78 (dt, 1H); 5.68 (dt, 1H); 5.25 (s, 2H).

5-amino-2-bromophenol (2d). 74% yield. ¹H NMR (CDCl₃) δ 7.19 (d, 1H); 6.39 (d, 1H); 6.20 (dd, 1H); 5.39 (s, 1H); 3.72 (s, 2H).

3-amino-2-chlorophenol (2e). Quantitative yield. ¹H NMR (CDCl₃) δ 6.98 (t, 1H); 6.45 (dd, 1H); 6.38 (dd, 1H); 5.44 (s, 1H); 4.05 (s, 2H).

3-amino-5-chlorophenol (2f). 55% yield. ¹H NMR (d₆-DMSO) δ 9.32 (s, 1H); 6.02 (d, 1H); 5.92 (d, 2H); 5.27 (s, 2H).

3-amino-5-(trifluoromethyl)phenol (2g). Quantitative yield. ¹H NMR (d₆-DMSO) δ 9.80 (s, 1H); 6.73 (s, 2H); 6.46 (s, 1H); 6.39 (s, 1H); 6.53 (s, 1H).

3-amino-2,6-difluorophenol (2h). 87% yield. ¹H NMR (d₆-DMSO) δ 9.67 (s, 1H); 6.67 (m, 1H); 6.15 (m, 1H); 4.87 (s, 2H).

General procedure for aryl azide formation. Aniline (2 mmol) was dissolved in 4 mL of AcOH. Tetrafluoroboric acid etherate (0.8 mL, 6 mmol) was added, followed by sodium nitrite (0.2 g, 3 mmol) in three portions over 30 min. The mixture was added dropwise to 40 mL of vigorously stirring Et₂O at 0° C. The resulting light brown precipitate was collected by filtration, then used in the next step without further purification. Sodium azide (0.13 g, 4 mmol) was dissolved in 20 mL of H₂O at 0° C. The diazonium from step 1 was added, followed by the addition of 20 mL of EtOAc, then the reaction was stirred to RT over 18 hr. The reaction was extracted 3X with 25 mL of EtOAc. The organic fractions were combined, washed 2X with 10 mL of brine, then dried with MgSO₄, filtered, and concentrated.

3-azido-5-fluorophenol (3b). 76% yield. ¹H NMR (D₆-acetone) δ 9.57 (s, 1H); 6.39 (m, 3H).

3-azido-4-fluorophenol (3c). 71% yield. ¹H NMR (CDCl₃) δ 6.98 (t, 1H); 6.56 (m, 2H); 4.87 (s, 1H).

5-azido-2-chlorophenol (3d). 62% yield. ¹H NMR (CDCl₃) δ 7.32 (d, 1H); 6.73 (d, 1H); 6.59 (dd, 1H); 5.63 (s, 1H).

3-azido-2-fluorophenol (3e). 40% yield. ¹H NMR (CDCl₃) δ 6.99 (m, 1H); 6.80 (m, 1H); 6.67 (m, 1H); 5.25 (s, 1H).

5-azido-2-bromophenol (3f). 31% yield. ¹H NMR (CDCl₃) δ 7.43 (d, 1H); 6.73 (d, 1H); 6.54 (dd, 1H); 5.60 (s, 1H).

3-azido-2-chlorophenol (3g). 60% yield. ¹H NMR (CDCl₃) δ 7.22 (t, 1H); 6.84 (dd, 1H); 6.80 (dd, 1H); 5.70 (s, 1H).

5-azido-2-methylphenol (3h). 29% yield. ¹H NMR (CDCl₃) δ 7.09 (d, 1H); 6.56 (dd, 1H); 6.49 (d, 1H); 5.36 (s, 1H); 2.23 (s, 3H).

3-azido-2-methylphenol (3i). 20% yield. ¹H NMR (CDCl₃) δ 7.12 (t, 1H); 6.77 (d, 1H); 6.60 (d, 1H); 4.78 (s, 1H); 2.13 (s, 3H).

3-azido-5-chlorophenol (3j). 72% yield. ¹H NMR (CDCl₃) δ 6.65 (d, 2H); 6.42 (t, 1H); 5.10 (s, 1H).

3-azido-5-(trifluoromethyl)phenol (3k). 15% yield. ¹H NMR (d₆-DMSO) δ 10.52 (s, 1H); 6.87 (s, 1H); 6.84 (s, 1H); 6.77 (s, 1H).

3-azido-2,6-difluorophenol (3l). 13% yield. ¹H NMR (CDCl₃) δ 6.91 (m, 1H); 6.60 (m, 1H); 5.56 (s, 1H).

3-azido-2-chloro-6-methylphenol (3m). 86% yield. ¹H NMR (CDCl₃) δ 7.06 (d, 1H); 6.70 (d, 1H); 5.77 (s, 1H); 2.28 (d, 3H).

N-(5-chloro-2-methylphenyl)propiolamide. Propiolic acid (7 g, 0.1 mol) was dissolved in acetonitrile (400 mL) then cooled to 0° C. DCC (22.7 g, 0.11 mol) was added, followed by **4** (21.24 g, 0.15 mol), then the reaction was stirred to RT over 18 hr. The precipitated DCU was removed by filtration, then the clear solution was concentrated. The crude solid was washed with hexanes, followed by DCM. Additional product was precipitated from the DCM fraction at 0° C. The product was combined and dried to give 12.57 g of **5** (65% yield). ¹H NMR (CDCl₃) δ 7.99 (s, 1H); 7.12 (q, 2H); 2.99 (s, 1H); 2.29 (s, 3H).

General procedure for triazole coupling. Starting azide (3a-i) (1 mmol), **5** (0.19 g, 1 mmol), CuSO₄·5 H₂O (25 mg, 0.1 mmol), and sodium ascorbate (0.1 g, 0.5 mmol) were dissolved in 5 mL of EtOH. The reaction was refluxed for 18 hr at 80° C. After cooling to RT the reaction mixture was diluted with 10 mL of 50% EtOH/50% H₂O, then the resulting precipitate was collected by filtration.

N-(5-chloro-2-methylphenyl)-1-(4-fluoro-3-hydroxyphenyl)-1H-1,2,3-triazole-4-carboxamide (TR001). 76% yield. ¹H NMR (d₆-DMSO) δ 10.10 (s, 1H); 9.37 (s, 1H); 7.62 (d, 1H); 7.58 (d, 1H); 7.41 (d, 2H); 7.32 (d, 1H); 7.24 (dd, 1H); 2.77 (s, 3H).

N-(5-chloro-2-methylphenyl)-1-(3-fluoro-5-hydroxyphenyl)-1H-1,2,3-triazole-4-carboxamide (TR002). 30% yield. ¹H NMR (d₆-DMSO) δ 10.65 (s, 1H); 10.17 (s, 1H); 9.47 (s, 1H); 7.61 (s, 1H); 7.39 (d, 1H); 7.32 (m, 2H); 7.24 (t, 1H); 6.75 (d, 1H); 2.74 (s, 3H).

N-(5-chloro-2-methylphenyl)-1-(2-fluoro-3-hydroxyphenyl)-1H-1,2,3-triazole-4-carboxamide (TR003). 62% yield. ¹H NMR (d₆-DMSO) δ

FULL PAPER

10.68 (s, 1H); 10.18 (s, 1H); 9.19 (s, 1H); 7.61 (s, 1H); 7.33 (t, 1H); 7.24 (m, 4H); 2.28 (s, 3H).

***N*-(5-chloro-2-methylphenyl)-1-(2-fluoro-5-hydroxyphenyl)-1*H*-1,2,3-triazole-4-carboxamide (TR004)**. 71% yield. ¹H NMR (d₆-DMSO) δ 10.18 (s, 1H); 10.13 (s, 1H); 9.17 (d, 1H); 7.60 (s, 1H); 7.44 (t, 1H); 7.36 (d, 1H); 7.23 (m, 2H); 7.00 (m, 1H); 2.27 (s, 3H).

***N*-(5-chloro-2-methylphenyl)-1-(2,4-difluoro-3-hydroxyphenyl)-1*H*-1,2,3-triazole-4-carboxamide (TR005)**. 61% yield. ¹H NMR (d₆-DMSO) δ 11.13 (s, 1H); 10.20 (s, 1H); 9.19 (s, 1H); 7.60 (s, 1H); 7.30 (d, 3H); 2.28 (s, 3H).

***N*-(5-chloro-2-methylphenyl)-1-(4-chloro-3-hydroxyphenyl)-1*H*-1,2,3-triazole-4-carboxamide (TR006)**. 96% yield. ¹H NMR (d₆-DMSO) δ 10.12 (s, 1H); 9.41 (s, 1H); 7.26 (s, 3H); 7.44 (s, 1H); 7.32 (d, 1H); 7.24 (d, 1H); 2.51 (s, 3H).

***N*-(5-chloro-2-methylphenyl)-1-(2-chloro-3-hydroxyphenyl)-1*H*-1,2,3-triazole-4-carboxamide (TR007)**. 85% yield. ¹H NMR (d₆-DMSO) δ 11.01 (s, 1H); 10.18 (s, 1H); 9.17 (s, 1H); 7.62 (s, 1H); 7.39 (m, 1H); 7.32 (m, 1H); 7.24 (m, 2H); 7.18 (m, 1H); 2.28 (s, 3H).

***N*-(5-chloro-2-methylphenyl)-1-(3-chloro-5-hydroxyphenyl)-1*H*-1,2,3-triazole-4-carboxamide (TR008)**. 82% yield. ¹H NMR (d₆-DMSO) δ 10.65 (s, 1H); 10.16 (s, 1H); 9.48 (s, 1H); 7.60 (d, 2H); 7.42 (s, 1H); 7.32 (d, 1H); 7.24 (d, 1H); 6.98 (s, 1H); 2.27 (s, 3H).

1-(4-bromo-3-hydroxyphenyl)-*N*-(5-chloro-2-methylphenyl)-1*H*-1,2,3-triazole-4-carboxamide (TR009). 81% yield. ¹H NMR (d₆-DMSO) δ 11.03 (s, 1H); 10.16 (s, 1H); 9.43 (s, 1H); 7.74 (d, 1H); 7.60 (m, 2H); 7.38 (d, 1H); 7.32 (d, 1H); 7.24 (m, 1H); 2.27 (s, 3H).

***N*-(5-chloro-2-methylphenyl)-1-(2-chloro-3-hydroxy-4-methylphenyl)-1*H*-1,2,3-triazole-4-carboxamide (TR010)**. 90% yield. ¹H NMR (d₆-DMSO) δ 10.14 (s, 1H); 9.90 (s, 1H); 9.12 (s, 1H); 7.62 (d, 1H); 7.32 (d, 2H); 7.24 (dd, 1H); 7.14 (d, 1H); 2.32 (s, 3H); 2.28 (s, 3H).

***N*-(5-chloro-2-methylphenyl)-1-(3-hydroxy-4-methylphenyl)-1*H*-1,2,3-triazole-4-carboxamide (TR011)**. 65% yield. ¹H NMR (d₆-DMSO) δ 10.11 (s, 1H); 10.05 (s, 1H); 9.34 (s, 1H); 7.62 (s, 1H); 7.41 (s, 1H); 7.31 (m, 3H); 7.23 (d, 1H); 2.27 (s, 3H); 2.19 (s, 3H).

***N*-(5-chloro-2-methylphenyl)-1-(3-hydroxy-2-methylphenyl)-1*H*-1,2,3-triazole-4-carboxamide (TR012)**. 85% yield. ¹H NMR (d₆-DMSO) δ 10.12 (s, 1H); 10.10 (s, 1H); 9.07 (s, 1H); 7.63 (d, 1H); 7.32 (d, 1H); 7.24 (m, 2H); 7.05 (d, 1H); 6.95 (d, 1H); 2.28 (s, 3H); 1.93 (s, 3H).

***N*-(5-chloro-2-methylphenyl)-1-(3-(trifluoromethyl)-5-hydroxyphenyl)-1*H*-1,2,3-triazole-4-carboxamide (TR013)**. 32% yield. ¹H NMR (d₆-DMSO) δ 10.89 (s, 1H); 10.19 (s, 1H); 9.60 (s, 1H); 7.84 (s, 1H); 7.73 (s, 1H); 7.61 (s, 1H); 7.33 (d, 1H); 7.24 (m, 2H); 2.28 (s, 3H).

Biological evaluation, in vitro studies

Reagents. General reagents were from Sigma-Aldrich or Fisher. CsA, phenylarsine oxide, diamide, *N*-ethylmaleimide, carbonyl cyanide-4-(trifluoromethoxy)phenylhydrazone (FCCP) were from Sigma-Aldrich, digitonin was from Acros organics, rhodamine 123 (Rh123) and Calcium Green-5N were from ThermoFisher Scientific, copper-*o*-phenanthroline was prepared just before use by mixing CuSO₄ with *o*-phenanthroline at a 1:2 molar ratio in double-distilled water.

Plasma stability determination. The degradation of TR001 in the presence of mouse plasma (from Innovative Research) was used to predict the plasma stability of the compound to esterase catalyzed hydrolysis. A positive control for plasma cholinesterase, propantheline bromide, was included in all assays. Briefly, murine plasma was incubated with 1 μM TR001. Aliquots were removed at t=0, 5, 15, 30, and 60 and 120 min and quenched with acetonitrile containing structurally related compound (TR073) as the internal standard. The amount of TR001 remaining in the supernatant was assessed by LC-MS/MS in multiple reaction monitoring mode (MRM) using a 4000 QTRAP (SCIEX) with electrospray ionization source. The instrument was operated in negative mode with source parameters: source voltage -4500 kV, GS1 50, GS2 50, CUR 30, TEM 650 and CAD gas MED. Optimal MRM transitions were obtained by direct infusion of the pure compound into the source. The mass spectrometer was interfaced to a Shimadzu (Columbia, MD) SIL-20AC XR auto-sampler maintained at 35 °C followed by 2 LC-20AD XR LC pumps. The internal standard and compound of interest were resolved

using a Gemini-NX C18 50x2.1 mm column (Phenomenex) with 0.1% formic acid (solvent A) and 0.1% formic acid in acetonitrile (solvent B). The injection volume was 10 μL at a flow rate of 0.75 mL/min. The gradient elution was 10% B to 95% B over 5 min and held at 95% for 1 min before returning to start conditions. The column was maintained at 40°C using a Shimadzu CTO-20AC column oven. Data were acquired using Analyst 1.6.2 and analyzed using MultiQuant 3.0.1 software. The first-order rate constant for substrate depletion was determined from a linear least squares fit of the natural log of the percent parent compound remaining versus time. The rate constant was used to calculate the plasma half-life as an indicator of stability.

Mouse studies. All procedures were approved by the Institutional Animal Care and Use Committee (IACUC) at Oregon Health and Science University (IP00000689 to M.F.).

Isolation of mitochondria. C57BL6/N mouse liver mitochondria were prepared from 2 to 6 month old male mice by standard differential centrifugation. Mice fed *ad libitum* were euthanized with CO₂ followed cervical dislocation, their livers were excised and placed in a glass beaker containing ice-cold isolation buffer (IB: 0.25 M sucrose, 10 mM Tris-HCl, 0.1 mM EGTA-Tris, pH 7.4) supplemented with fatty acid free bovine serum albumin. Livers were then cut into small pieces with scissors, rinsed with ice-cold IB, and passed through a pre-chilled Potter homogenizer with Teflon pestle. The homogenate (~ 30 mL per liver) was transferred to centrifuge tubes, and unbroken cells and nuclei were removed by centrifugation at 700 g for 10 min at 4 °C. The supernatant containing mitochondria and other organelles was transferred to new tubes and centrifuged at 6000 g for 10 min at 4 °C. The resulting supernatant was discarded and mitochondrial pellet was carefully suspended in ice-cold IB and spun at 9500 g for 5 min at 4°C. The pellet was suspended in IB to give a protein concentration of ~ 60–80 mg/mL and stored on ice. Experiments were started immediately and completed within 5 h. Protein concentration was determined by the Biuret method.

Assessment of mitochondrial swelling. Changes in mitochondrial volume of isolated mouse liver mitochondria were followed in a 96-well clear assay plate at a final volume of 0.2 mL and 0.25 mg/mL mitochondrial protein. Absorbance was read for 30 min at 540 nm on a Tecan Infinite F200 plate reader. Activity of test compounds was addressed as follows: First, 0.1 mL of sucrose assay buffer (SAB: 0.250 M sucrose, 10 mM MOPS-Tris, 0.01 mM EGTA-Tris, 1.0 mM phosphoric acid-Tris, 10 mM glutamate and 5 mM malate, pH 7.4) supplemented with twice the CaCl₂ concentration required to induce mitochondrial swelling (which was determined for each preparation of mitochondria, typically 50 μM) was dispensed to the assay plate. A set of wells also contained 2.0 mM EGTA (to prevent mitochondrial swelling). The test wells contained a range of concentrations (in 1:2 serial dilutions) of the compounds of interest or 2% DMSO. Experiments were started by the addition of 0.1 mL of mitochondrial suspension (0.5 mg/mL mitochondria in SAB without respiratory substrates) to the assay plates. EC₅₀ ± SE were determined with OriginPro software by applying Hill1 function fitting algorithm on average concentration response data of n=3-41 independent preparations.

Assessment of mitochondrial membrane potential. Mitochondrial membrane potential – to evaluate toxicity – of isolated mouse liver mitochondria was assessed based on fluorescence quenching of the cationic fluorescent dye Rh123 upon its accumulation into mitochondrial matrix due to inside negative membrane potential. Compounds that interfere with the build-up or maintenance of IMM potential would shift Rh123 fluorescence to higher values compared to DMSO treated samples. Uncoupler FCCP was used to account for nonspecific fluorescence. First, 0.1 mL of SAB was dispensed to a 96-well black assay plate. A set of wells also contained 0.8 μM FCCP (to prevent Rh123 uptake). The test wells contained a range of concentrations (in 1:2 serial dilutions) of the compounds of interest or 2% DMSO. Then, 0.1 mL of 0.5 mg/mL mitochondria in SAB devoid of respiratory substrates but supplemented with 0.8 μM Rh123 were added to all wells of the assay plate. Fluorescence intensity (ex/em 485/535 nm) was read on a Tecan Infinite F200 plate reader for 7 min and value at 5 min was considered for analysis. EC₅₀ ± SE were determined with OriginPro software by applying Hill1 function fitting algorithm on average concentration response data of n=3 independent preparations.

FULL PAPER

Assessment of Ca²⁺ retention capacity (CRC). CRC of isolated mouse liver mitochondria was assessed as follows: First, 0.1 mL of SAB were dispensed to a 96-well black assay plate in the presence of 2% DMSO (control wells) or varying concentrations of test compounds, in 1:2 serial dilutions. Then, 0.1 mL of 0.5 mg/mL mitochondria in SAB devoid of respiratory substrates, but supplemented with 1 μ M Calcium Green-5N were added to all wells of the assay plate. A train of 10 μ M CaCl₂ pulses was added at 2 min intervals, and fluorescence intensity (ex/em 485/535 nm) was read on Tecan Infinite F200 plate reader.

Cell culture. HeLa and Hek293T cells were grown in Dulbecco's modified Eagle's medium (DMEM) supplemented with 10 % fetal bovine serum, 100 U/mL penicillin and 100 mg/mL streptomycin in a humidified atmosphere of 5% CO₂/95% air at 37 °C.

Generation of CyPD-null cells. The CRISPR/Cas9 system was used to create HEK293T lines lacking the expression of the gene, *Ppif*, encoding CyPD. The guide used for the CRISPR was CCGACCCGCGCCCGCATGC (TGG) which targets the second amino acid of the coding sequence. Following transfection, individual cell lines were selected and expanded as outlined in Antoniel et al.^[26]. Western blot analysis of selected clones indicated the absence of CyPD protein in several clones. Subsequent sequence analysis of these null clones indicated the introduction of an early frame shift mutation that halted protein expression.

CRC of permeabilized cells. Wild-type or CyPD-null HEK293T cells were cultured for 48 h to reach 70–80 % confluency, then harvested by trypsinization and washed in KCl buffer (KB: 0.13 M KCl, 10 mM MOPS-Tris, 1 mM phosphoric acid-Tris, 0.1 mM EGTA-Tris, pH 7.4). Cells were then suspended in KB (except that EGTA-Tris was increased to 1.0 mM) to 10⁶ cells/mL and treated with 0.1 mM digitonin for 10 min on ice to permeabilize the plasma membrane. Following excess digitonin elimination by washing cells twice in ice-cold KB, the cells were suspended to 2 x 10⁷ cells per mL in ice-cold KB containing 10 μ M EGTA-Tris and kept on ice. CRC was assessed in a black 96-well plate in a final volume of 0.2 mL and buffer containing 0.13 M KCl, 10 mM MOPS-Tris, 1 mM phosphoric acid-Tris, 0.01 mM EGTA-Tris, 5 mM glutamate, 2.5 mM malate and 0.5 μ M Calcium Green-5N. A train of 10 μ M Ca²⁺ pulses was added at 4 min intervals, and fluorescence intensity (ex/em 485/535 nm) was read on Tecan Infinite F200 plate reader.

Measurement of respiration. Mitochondrial oxygen consumption of isolated mitochondria or HeLa cell monolayer was assessed with the Seahorse Extracellular Flux Analyzer XF24 (Seahorse Bioscience, Billerica, MA, USA). Isolated mouse liver mitochondria: Mitochondrial assay solution contained 220 mM mannitol, 70 mM sucrose, 25 mM MOPS-Tris, 10 mM Pi-Tris, 5 mM MgCl₂, 1 mM EGTA-Tris, 0.2% fatty acid free BSA, 5 mM succinate and 2 μ M rotenone, pH 7.4. Mitochondria (5 μ g, suspended in 50 μ L mitochondrial assay solution) were added to each well of an XF24 cell culture microplate, centrifuged at 2000 g for 20 min at 4°C and then supplemented with 450 μ L of mitochondrial assay solution containing 4 mM ADP to initiate the experiments. Additions were as indicated in Figure 5 A.

HeLa cells: cells were seeded at a density of 3x10⁴ per well in 0.2 mL DMEM and cultured for 24 h. Assays were started by re-placing the growth medium with 0.5 mL serum and antibiotic-free unbuffered DMEM (pH 7.4) and additions were made as indicated in Figure 5 C.

Cell viability assay. HeLa cells were seeded at a density of 10⁴ per well in 96-well plates and let to adhere for 6 h before treatment with varying concentrations of **TR001** or vehicle (1% DMSO). After treatment for 24 h the relative viable cell number was determined with a CellTiter 96 Aqueous One Solution Cell Proliferation Assay Kit (Promega).

Biological evaluation, in vivo studies in zebrafish

Zebrafish studies. Wildtype adult zebrafish were maintained in the Zebrafish Facility of the Biology Department of the University of Padova in aerated saline water, which was continuously filtered by a circulating system, at 28.5°C with a precise light/dark cyclic conditions (14/10 hours), according to standard protocols^[27,28]. To obtain embryos for injection experiments, two or three females were paired with two or three males in a 1.5 litre tank and separated by a transparent wall until morning. The next

morning, the transparent wall was removed and the zebrafish were free for courtship and mating. Fertilized eggs were collected and kept in fish water, containing 0.5 mM NaH₂PO₄ (Sigma-Aldrich, S8282), 0.5 mM NaHPO₄ (Sigma-Aldrich, S7909) and 3 mg/L instant ocean (Instant Ocean, SS15-10), at 28.5°C. All procedures were approved by the OPBA of the University of Padova and authorized by the Italian Ministry of Health (415/2015).

Morpholino antisense injection and treatment. Knock-down of *col6a1* gene expression was obtained with a previously published morpholino^[25] with sequence GAG AGC GGA AGA ACC TTC ATT C (GeneTools, Inc.). A control morpholino with no sequence homology in the zebrafish genome was used in parallel (CCT CTT ACC TCA GTT ACA ATT TAT A). Zebrafish eggs from wild-type matings were injected at the 1-2 cell stage with approximately 10 nL of 0.1 mM morpholino solution (corresponding to 4 ng of morpholino) using a WPI pneumatic PicoPump PV820 injector (World Precision Instruments, Inc.). Zebrafish embryos were dechorionated at 20 hours post fertilization (hpf) and treated at 21 hpf with increasing doses (0.1, 1 and 10 μ M) of both **TR001** and **63** compounds dissolved in fish water with 1% DMSO (vehicle).

Motor activity. The number of spontaneous coiling events performed in 15 seconds by single zebrafish embryos was recorded at 24 hpf by light microscopy. Touch-evoked escape responses were recorded at 48 hpf by observing the ability of zebrafish embryos to escape after a tail-touch with a little tip. Embryos were subdivided in 4 groups according to the observed phenotype: paralyzed embryos, score 0; underdeveloped embryos showing only coiling events, score 1; embryos showing lower motility, score 2; normal embryos, score 3.

Survival. Zebrafish survival was monitored every 3 days for 30 days. Drug treatment with both **TR001** and **63** dissolved in fish water with 1% DMSO started at 21 hpf. After 3 days of treatment (4 days post fertilization, dpf), zebrafish were moved to a bigger tank (50 mL) with fresh compounds dissolved in 1% DMSO. As a control vehicle, fish water with 1% DMSO was used.

Birefringence. Muscle structure was monitored by birefringence analysis, taking advantage of muscle anisotropy, which is the ability of muscle fibers to refract polarized light. Briefly, zebrafish embryos at 48 hpf were anesthetized with 0.02% Tricaine (Sigma-Aldrich, E10521) and placed in 2% methylcellulose (Sigma-Aldrich, M0387) on a rectangular glass plate, which was positioned on the light path of a Leica M165FC stereomicroscope (Leica, Inc.). Two polarized filters were used, the first placed between the light source and the glass slide, light being refracted through muscle fibers; the second was placed above the zebrafish embryos and rotated at a 90° angle relative to the first filter. With this set-up, light refracted by muscle fibers (due to the pseudo-crystalline array of sarcomeres) is transmitted and analyzed. Integrated area of birefringence was calculated using ImageJ software. Birefringence values $\geq 3 \times 10^6$ pixels are typical of wild-type embryos, while values between 1 and 3 x 10⁶ pixels and values $\leq 1 \times 10^6$ pixels were taken to indicate a mild and severe myopathy, respectively^[25,29].

OCR measurement. The Seahorse XF-24 extracellular flux analyzer (Agilent Technologies, United States, California, Santa Clara) was used to measure oxygen consumption rate in *col6a1* zebrafish morphants at 48 hpf. One day prior to analysis, each well of the Seahorse XF-24 extracellular flux analyzer cartridge (Agilent Technologies, 101122-100) was filled with 1 mL of Seahorse XF Calibrant (Agilent Technologies, 100840-000) and placed at 37°C overnight. The day after, zebrafish embryos at 48 hpf were placed in a XF-24 islet capture microplate (one zebrafish per well). Each well was filled with 670 μ L of fish water and an islet capture screen was fixed on top of each well to prevent zebrafish from moving out of the measurement chamber. Subsequently, after calibration of the Seahorse XF 24 Extracellular Flux Analyzer cartridge, the XF-24 capture microplate was loaded in the Seahorse XF-24 Extracellular Flux Analyzer. First, basal respiration was measured. Second, respiration due to ATP synthase was measured after addition of 10 μ M oligomycin (Merck Millipore-495455). Third, maximal respiration capacity was measured by adding 2 μ M of the uncoupler carbonyl cyanide-4-(trifluoromethoxy)phenylhydrazone (FCCP, Sigma-Aldrich, C2920). Last, 1 μ M of the complex I inhibitor, rotenone (Sigma-Aldrich, R8875), and 1 μ M

FULL PAPER

of the complex III inhibitor, antimycin A (Sigma-Aldrich, A8674) were added to determine non-mitochondrial (residual) respiration.

Acknowledgements

The authors would like to thank Dennis Koop and Lisa Bieyle of the OHSU Bioanalytical/Pharmacokinetics Core for their assistance in the in assessing plasma stability of listed compounds. This work was funded by the Fondation Leducq (16CVD04).

Conflict of Interest.

The authors declare no conflicts of interest.

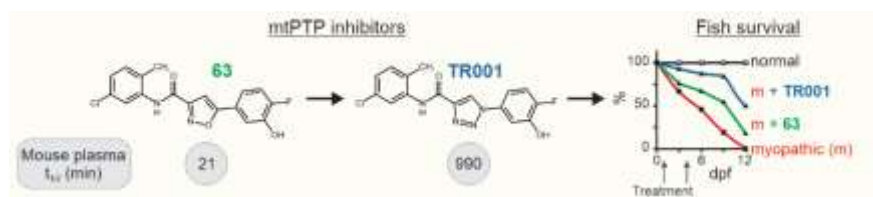
Keywords: calcium • click chemistry • inhibitors • mitochondria • muscular dystrophy • permeability transition pore

References:

- [1] G. Szabadkai, M. R. Duchon, *Physiology* **2008**, *23*, 84–94.
- [2] T. E. Gunter, S.-S. Sheu, *Biochim. Biophys. Acta - Bioenerg.* **2009**, *1787*, 1291–1308.
- [3] P. Bernardi, A. Krauskopf, E. Basso, V. Petronilli, E. Blalchy-Dyson, F. Di Lisa, M. A. Forte, *FEBS J.* **2006**, *273*, 2077–2099.
- [4] P. Bernardi, M. Forte, *Novartis Found. Symp.* **2007**, *287*, 157–64; discussion 164-9.
- [5] P. Bernardi, *Biochim. Biophys. Acta - Bioenerg.* **1996**, *1275*, 5–9.
- [6] L. Azzolin, S. von Stockum, E. Basso, V. Petronilli, M. A. Forte, P. Bernardi, *FEBS Lett.* **2010**, *584*, 2504–2509.
- [7] P. Bernardi, F. Di Lisa, *J. Mol. Cell. Cardiol.* **2015**, *78*, 100–106.
- [8] J. Šileikytė, E. Blalchy-Dyson, R. Sewell, A. Carpi, R. Menabo, F. Di Lisa, F. Ricchelli, P. Bernardi, M. Forte, *J. Biol. Chem.* **2014**, *289*, 13769–13781.
- [9] V. Giorgio, S. von Stockum, M. Antoniel, A. Fabbro, F. Fogolari, M. Forte, G. D. Glick, V. Petronilli, M. Zoratti, I. Szabo, et al., *Proc. Natl. Acad. Sci.* **2013**, *110*, 5887–5892.
- [10] J. Šileikytė, M. Forte, *Oxid. Med. Cell. Longev.* **2019**, *2019*, 1–11.
- [11] E. Basso, L. Fante, J. Fowlkes, V. Petronilli, M. A. Forte, P. Bernardi, *J. Biol. Chem.* **2005**, *280*, 18558–61.
- [12] S. Roy, J. Šileikytė, M. Schiavone, B. Neuenswander, F. Argenton, J. Aubé, M. P. Hedrick, T. D. Y. Chung, M. A. Forte, P. Bernardi, et al., *ChemMedChem* **2015**, *10*, 1655–1671.
- [13] S. Roy, J. Šileikytė, B. Neuenswander, M. P. Hedrick, T. D. Y. Chung, J. Aubé, F. J. Schoenen, M. A. Forte, P. Bernardi, *ChemMedChem* **2016**, *11*, 283–288.
- [14] B. W. Budzik, K. A. Evans, D. D. Wisnoski, J. Jin, R. A. Rivero, G. R. Szewczyk, C. Jayawickreme, D. L. Moncol, H. Yu, *Bioorg. Med. Chem. Lett.* **2010**, *20*, 1363–1367.
- [15] V. D. Filimonov, M. Trusova, P. Postnikov, E. A. Krasnokutskaya, Y. M. Lee, H. Y. Hwang, H. Kim, K.-W. Chi, *Org. Lett.* **2008**, *10*, 3961–3964.
- [16] V. Petronilli, P. Costantini, L. Scorrano, R. Colonna, S. Passamonti, P. Bernardi, *J. Biol. Chem.* **1994**, *269*, 16638–42.
- [17] P. Costantini, R. Colonna, P. Bernardi, *Biochim. Biophys. Acta - Bioenerg.* **1998**, *1365*, 385–392.
- [18] A. Zulian, J. Šileikytė, V. Petronilli, S. Bova, F. Dabbeni-Sala, G. Cargnelli, D. Rennison, M. a Brimble, B. Hopkins, P. Bernardi, et al., *Biochim. Biophys. Acta* **2011**, *1807*, 1600–5.
- [19] A. Zulian, M. Schiavone, V. Giorgio, P. Bernardi, *Pharmacol. Res.* **2016**, *113*, 563–573.
- [20] W. A. Irwin, N. Bergamin, P. Sabatelli, C. Reggiani, A. Megighian, L. Merlini, P. Braghetta, M. Columbaro, D. Volpin, G. M. Bressan, et al., *Nat. Genet.* **2003**, *35*, 367–371.
- [21] E. Palma, T. Tiepolo, A. Angelin, P. Sabatelli, N. M. Maraldi, E. Basso, M. A. Forte, P. Bernardi, P. Bonaldo, *Hum. Mol. Genet.* **2009**, *18*, 2024–2031.
- [22] A. Angelin, T. Tiepolo, P. Sabatelli, P. Grumati, N. Bergamin, C. Golfieri, E. Mattioli, F. Gualandi, A. Ferlini, L. Merlini, et al., *Proc. Natl. Acad. Sci. U. S. A.* **2007**, *104*, 991–6.
- [23] T. Tiepolo, a. Angelin, E. Palma, P. Sabatelli, L. Merlini, L. Nicolosi, F. Finetti, P. Braghetta, G. Vuagniaux, J. M. Dumont, et al., *Br. J. Pharmacol.* **2009**, *157*, 1045–1052.
- [24] W. R. Telfer, A. S. Busta, C. G. Bonnemann, E. L. Feldman, J. J. Dowling, *Hum. Mol. Genet.* **2010**, *19*, 2433–2444.
- [25] A. Zulian, E. Rizzo, M. Schiavone, E. Palma, F. Tagliavini, B. Blaauw, L. Merlini, N. M. Maraldi, P. Sabatelli, P. Braghetta, et al., *Hum. Mol. Genet.* **2014**, *23*, 5353–63.
- [26] M. Antoniel, K. Jones, S. Antonucci, B. Spolaore, F. Fogolari, V. Petronilli, V. Giorgio, M. Carraro, F. Di Lisa, M. Forte, et al., *EMBO Rep.* **2018**, *19*, 257–268.
- [27] C. B. Kimmel, W. W. Ballard, S. R. Kimmel, B. Ullmann, T. F. Schilling, *Dev. Dyn.* **1995**, *203*, 253–310.
- [28] A. Avdesh, M. Chen, M. T. Martin-Iverson, A. Mondal, D. Ong, S. Rainey-Smith, K. Taddei, M. Lardelli, D. M. Groth, G. Verdile, et al., *J. Vis. Exp.* **2012**, e4196.
- [29] M. Schiavone, A. Zulian, S. Menazza, V. Petronilli, F. Argenton, L. Merlini, P. Sabatelli, P. Bernardi, *Pharmacol. Res.* **2017**, *125*, 122–131.

FULL PAPER

Entry for the Table of Contents



Our first generation mitochondrial permeability transition pore (mtPTP) inhibitors, such as **63**, suffer from suboptimal mouse plasma stability. Herein we describe design, synthesis and in vitro characterization of a triazole-based second generation mtPTP inhibitors with significantly improved mouse plasma stability. Further, we validate the therapeutic potential of newly synthesized inhibitor **TR001** in a zebrafish model of muscular dystrophy.